# Highly Accelerated Dynamic Contrast-Enhanced MRI with Temporal Constrained Reconstruction

Huajun She, Rong-Rong Chen, Edward V. R. DiBella, Matthias Schabel, Leslie Ying, IEEE Senior Member

*Abstract*— **For DCE MRI applications, the images of adjacent time frames are often similar, especially when motion is minimal, in which case temporal TV is a reasonable regularization term. Temporal constraint reconstruction (TCR) has been developed to reconstruct dynamic images from undersampled k-t space data based on such prior information. However, the convergence speed of the algorithm highly depends on the initialization method. In this study, we study initialization using a composite high resolution image based on a jigsaw sampling pattern during pre-contrast frames. The proposed initialization method converges much faster than a conventional initialization method using low resolution images, especially at high reduction factors. In vivo breast imaging experiments were carried out to evaluate the performance of the proposed method. Experiments show the new initialization method allows TCR to achieve a high reduction factor up to 40 without compromising much of the spatial or temporal resolution. The reconstruction errors are much lower than those using the low resolution initialization when the same number of measurements is used.**

## I. Introduction

Dynamic Contrast Enhanced magnetic resonance imaging (DCE-MRI) of breast tumors provides a promising method to detect and characterize lesions. A contrast agent is injected and the data are acquired in *k*-space for each time frame. The acquired image series are used to track changes over time in the region of interest. By analyzing the time curve of uptake and washout, DCE-MRI can assist determine if the tumor is benign or malignant. In DCE-MRI, high spatial resolution is desirable to identify tumor location, and high temporal resolution can improve the accuracy of quantitative analysis of the uptake and washout curves [1]. However, there is usually a tradeoff between the spatial resolution and temporal resolution.

A number of techniques have been developed to enable the acquisition of images with both high spatial and temporal resolutions, such as keyhole [2], RIGR [3], UNFOLD [4], HYPR [5], k-t BLAST/k-t SENSE [6], and low rank methods [7-9]. Most of these methods acquire a fraction of *k*-space data in each time frame and reconstruct images using prior information to compensate for the information loss from reduced sampling. Recently, compressed sensing has emerged as another method to reconstruct dynamic images from undersampled data, which is based upon the principle that an image with a sparse representation in some transform domain can be recovered from randomly undersampled *k*-space data, using a nonlinear reconstruction [10]. Unlike k-t BLAST and k-t SENSE, compressed sensing does not require training data, so it may be less sensitive to inconsistencies between training data and practical data. Application of compressed sensing to dynamic MR imaging has been presented in methods such as k-t SPARSE [10], compressed sensing dynamic imaging [11], k-t FOCUSS [12], k-t ISD [13]. Often, temporal FFT is used as the sparsifying transform for cardiac cine images and PCA [14, 15] is used for images in parameter mapping. Temporal constraint reconstruction (TCR) method [16, 17] uses the temporal TV as the sparsifying transform. It assumes that the images of adjacent time frames are similar, especially when motion is minimal. Therefore, it is appropriate for DCE-MRI.

In this work, we investigate the application of TCR method in breast DCE-MRI to improve both the temporal and spatial resolution. In particular, we investigate how to choose the initialization such that the convergence speed is improved significantly. The proposed initialization method together with the corresponding sampling pattern is able to achieve a high reduction factor up to 40 without compromising much of the image quality or curve quantification.

## II. Method

In dynamic imaging, the imaging equation is written as

$$\mathbf{E}\mathbf{f}_t = \mathbf{d}_t, \tag{1}$$

where $\mathbf{d}_t$ is the vector formed from the acquired *k*-space data at time t, and $\mathbf{f}_t$ is the unknown image vector formed from the desired full field of view (FOV) image. The encoding matrix $\mathbf{E}$ consists of the Fourier transform, i.e.

$$\mathbf{E}_{m,n} = e^{-i2\pi \mathbf{k}_m \cdot \mathbf{r}_n}, \tag{2}$$

where $\mathbf{k}_m$ denote the coordinates of the *k*-space data. To reconstruct the desired image given knowledge of acquired data, TCR assumes that the images of adjacent time frames are similar, especially when motion is minimal, in which case temporal TV is used as a reasonable regularization term. The problem is formulated as a constrained nonlinear convex program based on Eq. (1):

$$\arg\min_{\mathbf{f}} \left\{ \sum_{t=1}^{T} \left\| \mathbf{d}_t - \mathbf{W}_t \mathbf{E}\mathbf{f}_t \right\|_2^2 + \alpha \mathrm{TV}(\mathbf{f}) \right\}, \tag{3}$$

This work is supported in part by the National Science Foundation CBET-1265612 and ECS-0547433

Huajun She and Rong-Rong Chen are with the Department of Electrical and Computer Engineering, University of Utah, Salt Lake City, UT 84112 USA. (email: huajun.she@utah.edu, rchen@eng.utah.edu)

Edward V. R. DiBella is with the Department of Radiology, University of Utah, Salt Lake City, UT 84108 USA. (email: edward.dibella@hsc.utah.edu)

Matthias Schabel is with Oregon Health Sciences University, Portland, OR 97239 USA. (email: schabelm@ohsu.edu).

Leslie Ying is with Department of Biomedical Engineering, Department of Electrical Engineering, The State University of New York at Buffalo, Buffalo, NY 14260 USA. (email: leiying@buffalo.edu)

978-1-4244-7929-0/14/$26.00 ©2014 IEEE

where $\mathbf{d}_t$ is the vector formed of the under-sampled *k*-space data acquired from the *t*-th frame, and $\mathbf{f}_t$ is the corresponding unknown image vector, $T$ is the total number of frames, f consists of images of all time frames, i.e. $\{f_1, f_2, \ldots, f_T\}$, $\mathbf{E}$ is the Fourier encoding matrix, $\mathbf{W}_t$ is the sparse sampling pattern of *k*-space data from the *t*-th frame, TV is the total variation operator along the temporal domain, $\alpha$ is regularization parameter which controls the tradeoff between the data consistency term and the prior information term. The temporal TV operator on a complex image series $\mathbf{f}$ is defined as:

$$\mathrm{TV}(\mathbf{f}) = \sum_{t=1}^{T} \left| \mathbf{f}_{t+1} - \mathbf{f}_t \right|, \qquad (4)$$

Gradient descent based method was used to implement the TCR method, which is regularly used for the minimization of an objective function. In [18], TCR is initialized using the low resolution images from the densely sampled ACS data at the central *k*-space. Such low resolution initialized TCR (LTCR) performs well in the cases where reduction factors are below 12. However, when the reduction factor goes higher, LTCR results in performance degradation.

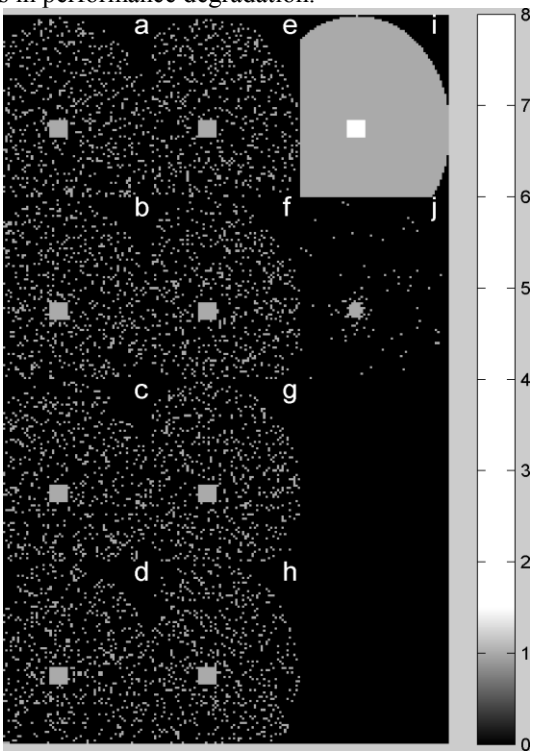


Figure 1. The pre-contrast frames sampling masks are shown in (a)-(h). Center ACS region is 8x8, and outer reduction factor is 8. The summation of the 8 downsampling masks (i) cover the entire *k*-space, and the central ACS region is covered 8 times. One of the post-contrast frame's mask with reduction factor R = 40 is shown in (j).

To improve the low resolution initialization, we propose a new initialization method using a composite image obtained from several frames. These frames are sampled with different jigsaw patterns and the sampled *k*-space data of these frames are combined along the temporal direction. Take the example in Fig. 1, the *k*-space data at ACS region are sampled in all frames and is thus averaged, and the outer *k*-space data from all frames are combined to generate a set of full *k*-space data. These full *k*-space data are then inverse Fourier transformed to obtain an initial estimation of a single image. This image is used as the initial estimation of all time frames. Then TCR is performed. We refer to the jigsaw initialized TCR reconstruction as JTCR.

## III. Experiment

Breast DCE-MRI data were acquired on a Siemens 3 Tesla scanner equipped with a seven channel dedicated breast coil. Two datasets from two study participants with clinically confirmed breast cancer were obtained under an institutional review board approved protocol. The root sum-of-squares (SOS) reconstruction from fully sampled data was used as the gold standard for visual comparison. All *k*-space data were acquired in full and then manually undersampled retrospectively to simulate accelerated scans.

The data were acquired using a 3D spoiled gradient echo pulse sequence with the following imaging parameters: TR = 3.16 ms, TE = 1.24 ms, flip angle = 10°. Omniscan of dose 0.1 ml/kg was injected at 4 mL/s followed by 20 ml saline flush injected at 2 mL/s. Temporal resolution was 12 s/frame with data acquired with 6/8 reduced Fourier space in the phase and slice directions and elliptical acquisition in the kx-ky plane. The acquisition matrices for the breast data kx × ky × kz × T are 256 × 83 × 64 × 45 and 256 × 83 × 64 × 42. The acquisition was bilateral, with the read direction left to right. The fast inverse Fourier transform (IFT) was performed in the read (kx) direction, and the ky-kz datasets were extracted from each slice in the x dimension.

The pre-contrast *k*-space center ACS region is about 8x8, and outer reduction factor is 8 for the first 8 pre-contrast images. The combination of the pre-contrast sampling patterns covers the entire outer *k*-space once, while the central ACS region is covered 8 times. We name the sampling pattern as the jigsaw sampling, whose union from several frames covers the entire *k*-space. The post-contrast *k*-space data is undersampled with variable-density random undersampling with the central *k*-space sampled with Nyquist rate as in [19]. Specifically, we choose samples randomly with sampling density scaling according to a power of distance from the *k*-space center. Undersampled *k*-space data were simulated by randomly picking a portion of the acquired phase encodes in the ky and kz directions. We have tried several reduction factors for the post-contrast frames, e.g. R = 40. The net reduction factor across all frames is around 24. An example of the jigsaw sampling masks over the first 8 pre-contrast frames is shown in Fig. 1 (a)-(h), the combined samples from 8 frames provide an elliptical partial Fourier acquisition of the *k*-space, as shown in Fig. 1 (i). An example of the variable density random sampling mask for a post-contrast frame is shown in Fig. 1 (j).

## IV. Results

All reconstructed images of the same dataset were normalized and shown individually on the same scale for visual evaluations of image quality. In case of the curves, all image series are normalized by dividing the mean value of the first frame's image, to make sure that the reconstructed images

are aligned at the beginning. Quantitative comparison was provided in terms of the normalized root mean squared error (nRMSE) with the SOS as the reference, which is defined as:

$$\mathrm{nRMSE} = \frac{\sqrt{\sum_{m=1}^{M}\sum_{n=1}^{N}\sum_{t=1}^{T}\left|\hat{f}(m,n,t) - f_{\mathrm{SOS}}(m,n,t)\right|^2}}{\max(f_{\mathrm{SOS}}) - \min(f_{\mathrm{SOS}})}, \qquad (5)$$

where $\hat{f}$ is the reconstructed image and $f_{\mathrm{SOS}}$ is the SOS image.

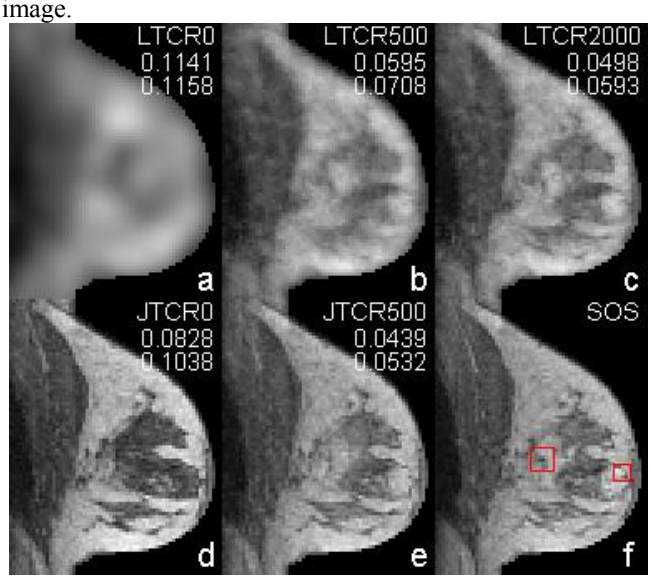


Figure 2. For the 1st dataset, reconstruction images of the last frame of LTCR for reduction factor R = 40, iteration number = 0, 500, 2000 (LTCR0, LTCR500, LTCR2000) are shown at (a), (b), (c). Reconstruction images for the last frame of JTCR for R = 40, iteration = 0, 500 (JTCR0, JTCR500) are shown at (d), (e). The SOS image of the last frame is shown in (f). The nRMSE of the last reconstructed frame (number at the top) and the average nRMSE of all reconstructed frames (number at the bottom) are shown in each subfigure. It shows that for the high reduction factor R=40, JTCR achieves superior performance to LTCR with much less number of iterations.

Fig. 2 compares the reconstructed images using TCR with jigsaw initialization (JTCR) and low resolution initialization (LTCR) for the first dataset. It is seen at high reduction factor of R=40, JTCR reconstruction with 500 iterations has much better resolution than LTCR reconstructions with 500 and even 2000 iterations. The JTCR reconstruction is close to SOS reconstruction visually. We also plot the mean signal intensity time curves for two different regions with breast lesions. The mean signal intensity time curves of JTCR in Fig. 3 are much closer to the SOS curves than those of LTCR do.

For the second dataset, Fig. 4 and Fig. 5 present the reconstructed images and the mean signal intensity time curves of two breast lesion regions using JTCR and LTCR. Similar to the observations of the first dataset, we see that at the high reduction factor of R=40, JTCR with 500 iterations yields a much sharper image than that of LTCR with 2000 iterations. The time curves of JTCR with 500 iterations are also much closer to the SOS curves compared to that of the LTCR curves with 2000 iterations.

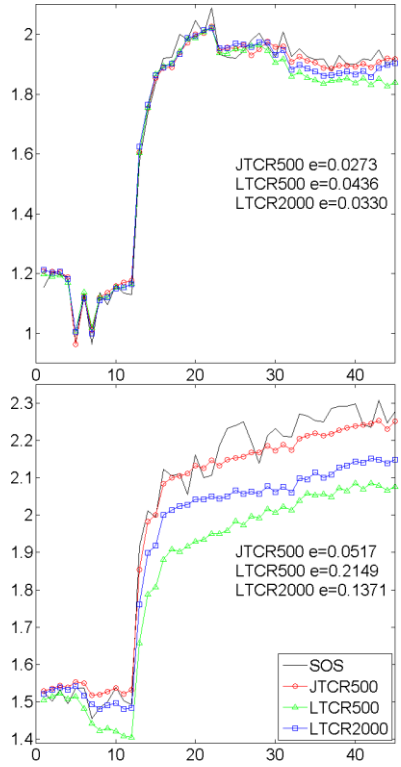


Figure 3. Comparisons the reconstructed time curves of SOS, JTCR500, LTCR500, and LTCR2000 for the 1st dataset. The x-axis represents the index of the time frame, and the y-axis represents the mean signal intensity. It shows that JTCR yields more accurate time curves than LTCR does at R = 40. The nRMSEs of the reconstructed curves compared with the SOS curves are shown in each figure.

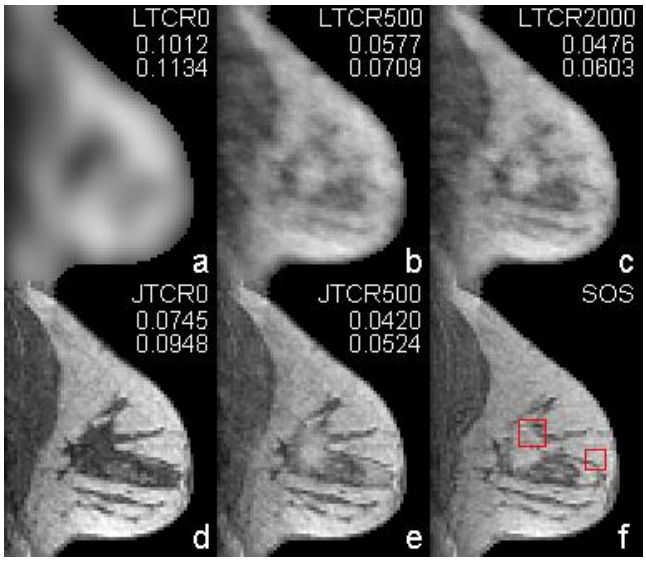


Figure 4. For the 2nd dataset, reconstruction images of the last frame of LTCR at reduction factor R = 40, iteration = 0, 500, 2000 (LTCR0, LTCR500, LTCR2000) are shown at (a), (b), (c). Reconstruction images for the last frame of JTCR iteration = 0, 500 (JTCR0, JTCR500) are shown at (d), (e). The SOS reconstruction of the last frame is shown in (f). The nRMSE of the last reconstructed frame (number at the top) and the average nRMSE of all reconstructed frames (number at the bottom) are shown in each subfigure. It shows that for high reduction factors, JTCR outperforms LTCR with much less number of iterations.

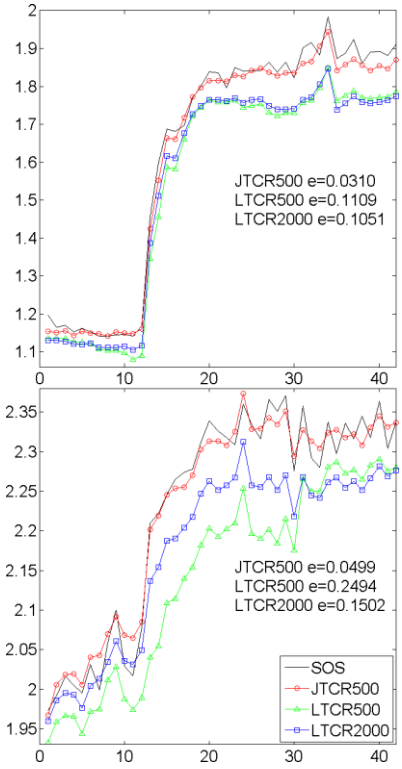


Figure 5. Comparisons of the reconstructed curves of SOS, JTCR500, LTCR500, and LTCR2000 for the 2nd dataset. It shows that at R = 40, JTCR yields better estimates of the time curves than LTCR does. The nRMSEs of the reconstructed curves compared with the SOS curves are also shown.

## V. Discussion

Since both the fidelity term and the temporal TV term are convex functions, the objective function of TCR is convex. In theory, it will eventually converge to the global optimal solution independent of the initial values. However, the initial guess using the low resolution image deviates from the SOS image so much that the algorithm needs many iterations to converge to the optimal solution. As we show in Figs. 2 and 4, the initial image of the jigsaw initialization is close to the SOS image, whereas the initial image of low resolution initialization is blurry. In addition, the number of unknown variables in TCR reconstruction is generally very large, which causes the algorithm to not converge until after several thousand iterations with low resolution initialization, especially at high reduction factors such as R=40. The jigsaw initialization converges quickly due to the better initialization which is close to the SOS image. As seen in the results, the JTCR outperforms LTCR at 500 iterations in both the visual quality of the image and the temporal curves. Although with 2000 iterations, the image quality of LTCR improves and the LTCR's curves move towards the SOS ones, LTCR is still inferior to JTCR while the running time is 4 times longer.

## VI. Conclusion

We study a new initialization method and sampling patterns to utilize high resolution images to initialize TCR. In vivo experimental results demonstrate that this initialization method and sampling patterns provide reconstructions superior to those using low resolution initialization visually and quantitatively.

## References


[1] T. Barrett, M. Brechbiel, M. Bernardo, and P. L. Choyke, "MRI of tumor angiogenesis," *J Magn Reson Imaging*, vol. 26, pp. 235–249, Aug. 2007.

[2] J. J. van Vaals, M. E. Brummer, W. T. Dixon, H. H. Tuithof, H. Engels, R. C. Nelson, B. M. Gerety, J. L. Chezmar, and J. A. den Boer, "Keyhole method for accelerating imaging of contrast agent uptake," *J Magn Reson Imaging*, vol. 3, pp. 671–675, July 1993.

[3] A. G. Webb, Z. P. Liang, R. L. Magin, and P. C. Lauterbur, "Applications of reduced-encoding MR imaging with generalized-series reconstruction (RIGR)," *J Magn Reson Imaging*, vol. 3, pp. 925–928, Nov. 1993.

[4] B. Madore, G. H. Glover, and N. J. Pelc, "Unaliasing by Fourier-encoding the Overlaps using the temporaL Dimension (UNFOLD), applied to cardiac imaging and fMRI," *Magn Reson Med*, vol. 42, pp. 813–828, Nov. 1999.

[5] C. A. Mistretta, O. Wieben, J. Velikina, W. Block, J. Perry, Y. Wu, K. Johnson, and Y. Wu, "Highly constrained backprojection for time-resolved MRI," *Magn Reson Med*, vol. 55, pp. 30–40, Jan. 2006.

[6] J. Tsao, P. Boesigner, and K. P. Pruessmann, "k-t BLAST and k-t SENSE: dynamic MRI with high frame rate exploiting spatiotemporal correlations," *Magn Reson Med*, vol. 50, pp. 1031–1042, Nov. 2003.

[7] S. Lingala, Y. Hu, E. V. R. DiBella, and M. Jacob, "Accelerated dynamic MRI exploiting sparsity and low-rank structure: k-t SLR," *IEEE Trans Med Imaging*, vol. 30, pp. 1042–1054, May 2011.

[8] J. P. Haldar and Z. P. Liang, "Low-rank approximations for dynamic imaging," in *Proc. IEEE Int Symp Biomed Imaging*, Chicago, 2011, pp. 1052–1055.

[9] T. Zhang, M. T. Alley, M. Lustig, X. Li, J. M. Pauly, and S. S. Vasanawala, "Fast 3D DCE-MRI with sparsity and low-rank enhanced SPIRiT (SLR-SPIRiT)," in *Proc. 21st Annual Meeting ISMRM*, Salt Lake City, 2013, pp. 2624.

[10] M. Lustig, J. M. Santos, D. L. Donoho, and J. M. Pauly, "k-t SPARSE: high frame rate dynamic MRI exploiting spatio-temporal sparsity," in *Proc. 14th Annual Meeting of ISMRM*, Seattle, 2006, pp. 2420.

[11] U. Gamper, P. Boesiger, and S. Kozerke, "Compressed sensing in dynamic MRI," *Magn Reson Med*, vol. 59, pp. 365–373, Feb. 2008.

[12] H. Jung, K. Sung, K. S. Nayak, E. Y. Kim, and J. C. Ye, "k-t FOCUSS: a general compressed sensing framework for high resolution dynamic MRI," *Magn Reson Med*, vol. 61, pp. 103–116, Jan. 2009.

[13] D. Liang, E. V. R. DiBella, R.-R. Chen, L. Ying, "k-t ISD: dynamic cardiac MR imaging using compressed sensing with iterative support detection", Magnetic Resonance in Medicine, vol. 68, pp. 41-53, July 2012.

[14] H. Pedersen, S. Kozerke, S. Ringgaard, K. Nehrke, and W. Y. Kim, "k-t PCA: Temporally Constrained k-t BLAST Reconstruction Using Principal Component Analysis," *Magn Reson Med*, vol. 62, pp. 706–716, Sep. 2009.

[15] L. Feng, R. Otazo, H. Jung, J. H. Jensen, J. C. Ye, D. K. Sodickson, and D. Kim, "Accelerated Cardiac T2 Mapping using Breath-hold Multiecho Fast Spin-Echo Pulse Sequence with k-t FOCUSS," *Magn Reson Med*, vol. 65, pp. 1661–1669, June 2011.

[16] G. Adluru, S. P. Awate, T. Tasdizen, R. T. Whitaker, and E. V. R. DiBella, "Temporally constrained reconstruction of dynamic cardiac perfusion MRI," *Magn Reson Med*, vol. 57, pp. 1027–1036, June 2007.

[17] G. Adluru, C. J. McGann, P. Speier, E. G. Kholmovski, A. Shaaban, and E. V. R. DiBella, "Acquisition and reconstruction of undersampled radial data for myocardial perfusion MRI," *J Magn Reson Imaging*, vol. 29, pp. 466-473, Feb. 2009.

[18] H. Wang, N. K. Bangerter, G. Adluru, M. Schabel, G. R. Morrell, and E. V. R. DiBella, "Comparison of highly accelerated TV and low rank methods for breast DCE data," in *Proc. 20th Annual Meeting ISMRM*, Melbourne, 2012, pp. 5194.

[19] M. Lustig, D. L. Donoho and J. M. Pauly, "Sparse MRI: The Application of Compressed Sensing for Rapid MR Imaging," *Magn Reson Med*, vol. 58, pp. 1182–1195, Dec. 2007.